Pacific Northwest
NATIONAL LABORATORY

PNNL-34887

Safe Electrolytes for Batteries

September 2023

Bingbin Wu
Witness Martin
Ruozhu Feng

U.S. DEPARTMENT OF ENERGY

Prepared for the U.S. Department of Energy
under Contract DE-AC05-76RL01830

DISCLAIMER

PACIFIC NORTHWEST NATIONAL LABORATORY
operated by
BATTELLE
for the
UNITED STATES DEPARTMENT OF ENERGY
under Contract DE-AC05-76RL01830

Printed in the United States of America

Available to DOE and DOE contractors from
the Office of Scientific and Technical Information,
P.O. Box 62, Oak Ridge, TN 37831-0062
www.osti.gov
ph: (865) 576-8401
fox: (865) 576-5728
email: reports@osti.gov

Available to the public from the National Technical Information Service
5301 Shawnee Rd., Alexandria, VA 22312
ph: (800) 553-NTIS (6847)
or (703) 605-6000
email: info@ntis.gov
Online ordering: http://www.ntis.gov

PNNL-34887

0BSafe Electrolytes for Batteries

September 2023

Bingbin Wu
Witness Martin
Ruozhu Feng

Prepared for
the U.S. Department of Energy
under Contract DE-AC05-76RL01830

Pacific Northwest National Laboratory
Richland, Washington 99354

Abstract

The demand for reliable and safe lithium-ion batteries (LIBs) for electric vehicles (EVs) and energy storage systems (ESS) necessitates the exploration of nonflammable phosphorus-based electrolytes as alternatives to the traditional flammable carbonate-based ones. However, integrating phosphorus-based electrolyte poses challenges, including capacity fading and compatibility issues with graphite material. Here, a high-throughput (HTP) electrochemical characterization method, similar to PH test paper, is introduced to fast screen compatible phosphorus-based electrolyte for use with graphite. Among 1,740 combinations of phosphorus-based electrolytes and graphite materials, 101 promising combinations are identified for further evaluation. These identified phosphorus-based electrolytes and graphite materials are evaluated and optimized in Li/Graphite half-cells and Graphite/$LiFePO_4$ (LFP) full-cells using commercial-level electrodes. The desolvation energy of a complex with one Li+ and four solvent molecules of phosphate or carbonate is calculated by density functional theory (DFT). Key parameters such as viscosity, ionic conductivity, and flammability of the electrolytes are thoroughly tested and optimized. The modified phosphate-dominant electrolyte (2 M LiFSI TEP/DME/EC (6/2/2, volume ratio) + 5 wt.% VEC + 5 wt.% FEC) demonstrates excellent thermal stability with lithiated graphite and showcases superior cycling performance in the Graphite/LFP full cell, surpassing prior research findings in phosphate-dominant electrolytes. By the rapid HTP screening and identification of compatible electrolyte-graphite combinations, this approach contributes to expediting the development of safer LIBs for EVs and ESS.

Summary

This study has introduced a HTP electrochemical characterization method and explored nonflammable phosphorus-based electrolytes as promising alternatives for LIBs. The HTP method, utilizing a Li/Graphite test electrode, enabled rapid screening and identification of potential electrolyte-graphite combinations. Among a large number of combinations screened, 101 were identified for further evaluation. Through extensive evaluation and optimization, the modified phosphate-dominant electrolyte, 2 M LiFSI TEP/DME/EC (6/2/2, v/v/v) + 5% FEC + 5% VEC, demonstrated superior cycling performance in Gr/LFP full cell configurations, surpassing previous research findings in developing phosphate-dominant electrolytes. The HTP electrochemical characterization method presented in this study offers a valuable tool for the efficient development of safe and efficient LIBs. In the future, integrating HTP viscosity and ionic conductivity tests with artificial intelligence (AI) vision inspection and machine learning technology will enhance the efficiency of this tool further. By rapidly screening electrolyte-graphite combinations, researchers and industry experts can expedite the discovery of optimal formulations while minimizing the risks associated with flammable electrolytes. While this work focused on the HTP screening method of electrolyte formulations, additional investigations into surface properties of graphite and the development of robust SEIs in phosphorus electrolytes should also be pursued to further enhance LIB performance and safety. The novel HTP electrochemical characterization method, combined with the exploration of nonflammable phosphorus-based electrolytes, represents a significant advancement in the development of safer and more efficient LIBs.

Acknowledgments

This research was supported by the Energy Storage Materials Initiative (ESMI), under the Laboratory Directed Research and Development (LDRD) Program at Pacific Northwest National Laboratory (PNNL). PNNL is a multi-program national laboratory operated for the U.S. Department of Energy (DOE) by Battelle Memorial Institute under Contract No. DE-AC05-76RL01830.

Contents

1.0 Introduction

The world is steadily transitioning from unsustainable, fossil fuel-based energy sources to cleaner, albeit intermittent, renewable sources for powering electric vehicles (EVs) and grid-level energy storage systems (ESS) in cities, homes, and office buildings.[1-3] Currently, lithium-ion batteries (LIBs) reign as the preferred battery technology for electric energy storage due to their lightweight nature, long cycle life, and high volumetric and gravimetric energy density metrics. By 2030, the estimated demand capacity of LIBs for EVs alone is projected to reach an astounding 8 terawatt-hours (TWh) and about 1 TWh for the stationary storage.[1] With such extensive implementation of lithium-ion batteries at the TWh level, ensuring the production of reliable and safe LIBs has emerged as a major concern for researchers, as mishandling or abuse can lead to rapid and catastrophic thermal failure.[4, 5] State-of-the-art LIBs commonly employ carbonate-based electrolytes, which possess a significant flammability risk, further exacerbating the potential for thermal runaway. In response to this challenge, researchers have extensively explored phosphorus-based alternatives since 2000 due to their nonflammable nature, high flash point, and wide liquid range.[6-8] Notable examples of phosphorus-based materials include trimethyl phosphate (TMP),9 triethyl phosphate (TEP),[10] and dimethyl methylphosphonate (DMMP).[11] However, even the addition of just 20 wt.% phosphate to a carbonate electrolyte leads to severe capacity fading in the graphite anode.7 Incorporating phosphate presents its own hurdle: it strongly coordinates with Li+ ions due to its high donor number (DN) and can readily intercalate into graphite layers in the absence of a robust solid electrolyte interface (SEI) film, resulting in graphite exfoliation.[12-14] To overcome this challenge, rational selection of graphite materials and SEI additives is crucial to ensure the proper functioning of graphite in a phosphate-dominant electrolyte. Wang .et al found that amorphous carbon-coated graphite demonstrates superior stability in 2 M $LiN(SO_2C_2F_5)_2$ TMP/γ-Butyrolactone (7/3, volume ratio) + 8 wt.% VEC + 2 wt.% VC +2 wt.% cyclohexane.[15] Despite the improved compatibility, the cycling capability remains limited to less than 10 cycles, even with a thin graphite electrode (~ 4.8 mg/cm^2). Studies have revealed that the compatibility between phosphate and graphite can be significantly enhanced in high concentrated electrolytes and localized high-concentration electrolyte (LHCE) due to the formation of Li^+-anion contact ion pairs (CIP) and aggregate clusters (AGGs) without free phosphate molecules.[12, 16, 17] However, these concentrated electrolytes contain only a small fraction (approximately 15 wt.% in LHCE) of phosphate, resulting in increased viscosity and reduced ionic conductivity.[18] Consequently, this impedes the effective utilization of commercially viable thick electrodes. In electrolytes dominated by phosphate, the compatibility between phosphate and graphite is influenced by several factors, including SEI additives, lithium salt, salt concentration, phosphate, cosolvents, graphite type and its surface properties,[15] rendering electrolyte design and optimization more complex and time-consuming.High-throughput (HTP) methods enable the rapid screening of potential electrolytes across diverse formulations.[19] One widely adopted approach is virtual screening, which employs HTP density functional theory (DFT) calculations or machine learning (ML) to establish quantitative structure-property relationships and predict novel materials.[20] While HTP electrolyte preparation can be accomplished using automated robotic systems,[21] the majority of HTP experimental

screening focuses on physical properties such as solubility, conductivity, and oxidative/reductive potentials.[22, 23] Unfortunately, there is a lack of reports on fast HTP electrochemical characterization of the compatibility between the electrolyte and active materials in LIBs. In this study, we introduce a Li/Graphite test electrode, akin to a "pH test paper", to facilitate HTP electrochemical characterization between graphite and nonflammable phosphorus-based electrolytes. Through this method, we successfully identified 101 combinations of phosphorus-based electrolytes and graphite materials out of a total of 1,740 combinations. It's important to note that by including additional graphite and electrolyte recipes, the number of combinations in this HTP method can be easily expanded to several thousand or more. Furthermore, we conducted further evaluation and optimization of the identified phosphate electrolytes and graphite in Li/Graphite half-cells and Graphite/$LiFePO_4$ (LFP) full-cells using commercial-level electrodes. The graphite/LFP full cell, utilizing the modified phosphate-dominant electrolyte (2 M LiFSI TEP/DME/EC (6/2/2, volume ratio) + 5 wt.% VEC + 5 wt.% FEC), exhibited superior cycling performance compared to previously published research. The novel HTP electrochemical characterization presented in this work offers a promising pathway to expedite the development of safe LIBs for future TWh-level EV and ESS applications.

2.0 Results and Discussion

2.1 HTP EL preparation and HTP electrochemical characterization

The utilization of advanced robotics and data exchange within the framework of Industry 4.0 has yielded machines that surpass human capabilities in executing repetitive tasks. In the domain of electrolyte preparation for LIBs, the achievement of precision necessitates the addition of multiple chemicals, including a lithium salt, 2-4 solvents, and 1-10 additives. This process is often protracted and laborious, particularly when generating numerous electrolytes for screening purposes. The HTP machine for electrolyte preparation liberates researchers from this monotonous procedure while maintaining utmost accuracy and efficiency. Figures 1a-1c illustrate the HTP machine employed in this study for nonaqueous electrolyte preparation.[24] To obviate contact with moisture and oxygen, the HTP robotic system was positioned within an Ar-filled glove box. Initially, the lithium salt and solid additives were dispensed into a 2 mL vial at the workstation depicted in Figure 1a. Subsequently, the solvents and liquid additives were injected through a separate workstation (Fig. 1b). The vial was then sealed and placed in an 8 * 6 vial tray, followed by shaking the tray to effect complete dissolution of the solids (Fig. 1c). By means of this methodology, a total of 290 phosphorus-based electrolytes were prepared, comprising eight phosphorus-based solvents (TMP, TEP, TPrP, TBP, DMMP, DEEP, DEMP, and DEPP, see Experimental procedure for full names), eight SEI additives (1,3-PS, DTD, FEC, $LiPO_2F_2$, VC, VEC, and DEVP), and four lithium salts ($LiPF_6$, LiFSI, LiDFOB, and LiBOB). The concentration of the lithium salt in each phosphorus-based electrolyte was maintained at 1.2 M. Additionally, a medium concentration of 2 M for LiFSI was prepared for comparative analysis. It is important to note that the addition of SEI additives was fixed at 10 wt.% and not optimized. Traditionally, the evaluation of compatibility between graphite anodes and electrolytes involves assembling Li/Graphite (Gr) half cells in a coin cell format. These cells are then subjected to galvanostatic charge/discharge cycling to determine if the graphite can achieve its normal capacity, which typically ranges from 330-360 mAh/g depending on the graphite source. For a graphite material, a minimum of 290 Li/Gr coin cells need to be assembled for the 290 phosphorus-based electrolytes prepared using a HTP machine. If multiple graphite materials are involved, the number of coin cells required increases linearly. In this study, we have selected six commercially available graphite materials (Fig.S1): 282863 (Sigma-Aldrich, Gr#1), TIMREX KS15 (TIMCAL, Gr#2), TIMREX SLP30 (TIMCAL, Gr#3), S360-M (BTR, Gr#4), FormulaBTTM SLC1520T (Superior Graphite, Gr#5), and Mage 3 (Hitachi, Gr#6). Consequently, a total of 1740 Li/Gr coin cells are necessary to complete the compatibility screening, which demands a substantial amount of time and testing equipment, making it unsuitable for HTP characterization. It is widely recognized that fully lithiated graphite undergoes a color transformation from black or grey to gold.[25] Based on this principle, we have designed a miniature Li/Gr test electrode (2 mm W * 7 mm L) consisting of a graphite electrode, a thin Li foil on a Cu foil, as shown in Figure. 1d. Immersing the Li/Gr test electrode in an electrolyte (Fig. 1e) triggers the spontaneous flow of electrons from the Li foil to the graphite electrode through the Cu substrate, while Li+ ions transport through the electrolyte and intercalate into the graphite layers, converting the graphite into a LiC_6 composite. If the electrolyte is compatible with graphite, the graphite will exhibit a golden color within 6-12 hours. Conversely, an incompatible electrolyte will not induce this color change (Fig. 1e). Multiple Li/Gr test electrodes, incorporating various graphite sources, can be immersed in the electrolyte as needed (Fig. 1f), enabling fast HTP electrochemical characterization of the electrolytes and graphite materials. Figure 1g displays the pristine Li/Gr test electrodes containing six graphite materials (Gr#1-Gr#6). After immersion in the traditional carbonate electrolyte, 1 M $LiPF_6$ EC/DEC/EMC (1/1/1, v/v/v) + 1 wt.% VC + 5 wt.% FEC, all Li/Gr test electrodes exhibit a gold color within 6 hours (Fig. 1h), confirming the viability of the

developed HTP characterization method. However, when immersed in a phosphorus-based electrolyte, such as 1.2 M LiFSI TEP + 10 wt.% 1,3-PS, only Gr#2 exhibits a dark gold color and Gr#1 displays partial gold coloration, while Gr#3-Gr#6 show no color change (Fig. 1i), indicating the significance of graphite selection. Substituting the SEI additive 1,3-PS with FEC results in partial gold coloration for Gr#3-Gr#5 (Fig. 1j), highlighting the crucial role of the SEI additive in stabilizing phosphorus-based electrolyte with graphite. By increasing the lithium salt concentration to a medium concentration of 2 M, most graphite materials, except Gr#6, exhibit a positive effect and partial gold coloration (Fig. 1k). Further increasing the concentration to 3 M results in complete gold coloration for all graphite materials (Fig. 1l), similar to the traditional carbonate electrolyte (Fig. 1h), consistent with the published report indicating the compatibility of high-concentration phosphate electrolyte with graphite.[17] Thus, the developed Li/Gr test electrode offers a rapid and reliable method to characterize the electrochemical compatibility between phosphorus-based electrolytes and graphite materials, facilitating integration into HTP electrolyte screening.Figure 2a presents a summary of the color change results for six as-developed Li/Gr test electrodes in each of the 290 phosphorus-based electrolytes. These results are organized into a matrix, consisting of 38 rows (S1-S38) representing eight solvents, four lithium salts, and two concentrations for LiFSI. The matrix also contains 48 columns (A1-A48) representing six different Li/Gr test electrodes and eight SEI additives. As a result, any combination of graphite and phosphorus-based electrolyte can be denoted as SxxAxx. For example, S16A35 represents the combination of Li/Gr test electrode (Gr#5) and 1.2 M LiDFOB TBP + 10 wt.% VEC. If the SxxAxx in Figure 2a is displayed with a yellow background, it indicates a complete or partial color change to gold on the graphite of the Li/Gr test electrodes. It is important to note that even a small area of color change on the Li/Gr test electrode in an electrolyte, such as Gr#1 in 1.2 M LiFSI TEP + 10 wt.% 1,3-PS (Fig. 1i), is considered a positive result and marked with a yellow background. This approach ensures that the HTP screening will not miss any possibilities. Remarkably, within a short period of one week, including the production of 1740 Li/Gr test electrodes, we identified 101 positive combinations showing partial or complete gold coloration on the graphite. This outcome would have been impractical using traditional methods that involve assembling and testing at least 1740 Li/Gr coin cells. From the analysis of Figure 2a, the following key findings emerge: 1) Lithium borates with DEVP or LiFSI additives demonstrate higher compatibility with graphite in low concentration phosphorus-based electrolytes compared to $LiPF_6$ and LiFSI. This is attributed to the early reduction of borates (1.5-1.8 V vs Li/Li+), which occurs prior to solvent reduction (less than 1 V) at the graphite electrode (Fig. S2).[26, 27] 2) Increasing the LiFSI concentration to 2 M leads to more compatible combinations between graphite and phosphorus-based electrolytes. 3) Phosphate-based electrolytes (TEP, TBP) exhibit a higher likelihood of good compatibility with graphite than phosphonate-based electrolytes (DMMP, DEEP). The compatibility between graphite and phosphorus-based electrolytes is significantly influenced by the presence of free phosphorus-based molecules in the electrolyte, which can harm the stability of the SEI.[14] In general, a Li+ ion is more likely to coordinate with four ester solvent molecules in the electrolyte.[28] When considering the molar ratio of P:Li in 1.2 M and 2 M phosphorus-based electrolytes (Fig.2b), most low concentrations of 1.2 M phosphorus-based electrolytes exhibit a P:Li ratio above 4, particularly in phosphonate-based electrolytes. This indicates a higher presence of free phosphonate molecules in the electrolyte compared to phosphate-based electrolytes, posing challenges to SEI stability on graphite. In medium concentration 2 M phosphorus-based electrolytes, the ratio of free phosphorus-based molecules decreases, and anions will participate in direct coordination with Li+, resulting in a stable CIP-like mechanism in high concentration electrolytes.[29] By conducting DFT calculations on the desolvation energy of a Li+ ion and four solvent molecules (Fig.2c), it's found that the desolvation energy of Li^+ in a carbonate baseline electrolyte (1 M $LiPF_6$ EC/DEC/EMC (1/1/1, v/v/v) + 1 wt.% VC + 5 wt.% FEC) with an EC/DEC/EMC molar ratio of approximately 2:1:1, is -12.7 kcal/mol, which aligns

with previous literature.[30] However, the phosphorus-based solvents display 2-7 times higher desolvation energy than the carbonate solvents, making it more challenging for Li^+ to disengage from the phosphorus-based solvents before intercalation into graphite. This can result in co-intercalation of the phosphorus-based solvents into the graphite if a robust SEI does not exist.[14]

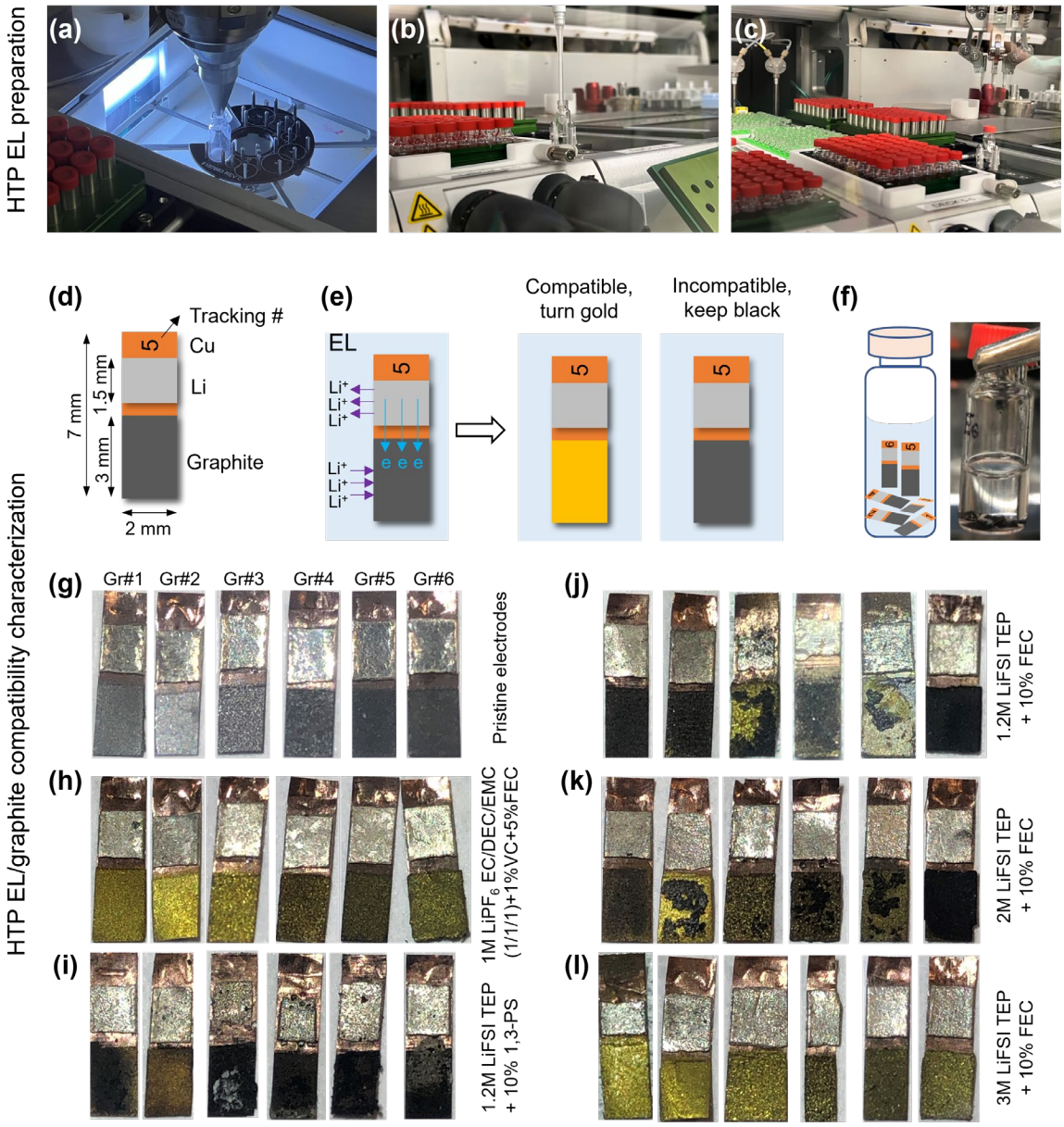

Figure 1. HTP electrolyte preparation and HTP electrochemical characterization of electrolytes and graphite materials. The HTP machine facilitated the electrolyte preparation process, utilizing three workstations: (a) for dispensing lithium salt and solid additives, (b) for injecting solvents and liquid additives, and (c) for sealing, shaking, and stirring the vial. A schematic graph of a Li/Gr test electrode for HTP EL screening is shown in (d), along with the working principle of the Li/Gr test electrode in (e). Additionally, (f) presents the schematic graph and photo of vials containing multiple Li/Gr test electrodes. Pristine Li/Gr test electrodes are depicted in (g), and subsequent images show the electrodes after soaking in various electrolyte formulations: (h) 1M LiPF6 EC/DEC/EMC (1/1/1, v/v/v%) + 1% VC + 5% FEC, (i) 1.2M LiFSI TEP + 10% 1,3-PS, (j) 1.2M LiFSI TEP + 10% FEC, (k) 2M LiFSI TEP + 10% FEC and (l) 3M LiFSI TEP + 10% FEC.

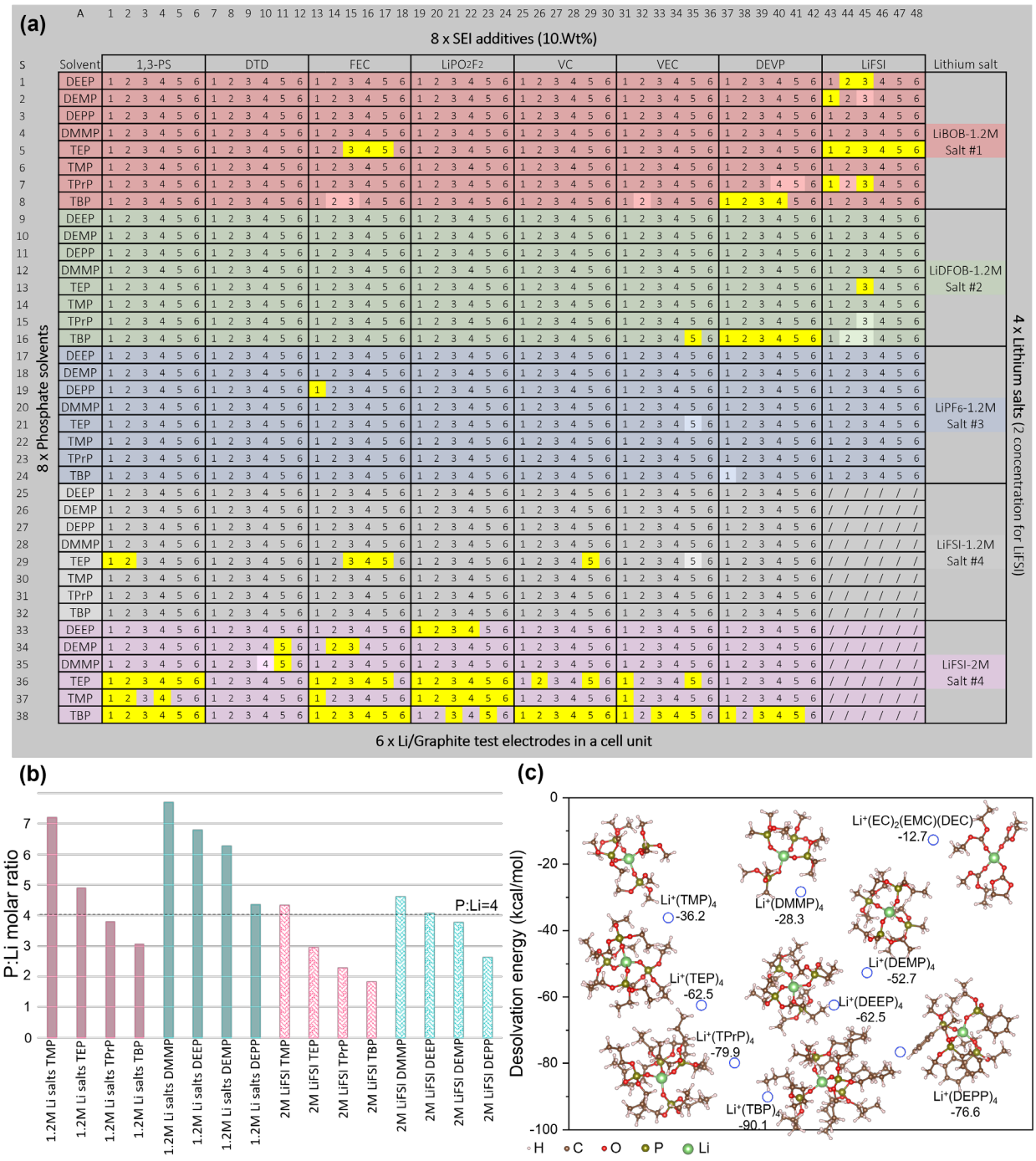

Figure 2. Color change of Li/Gr test electrodes in various phosphorus-based electrolytes prepared by HTP machine and electrolytes properties. (a) presents a summary of the color change results for six as-developed Li/Gr test electrodes immersed in 290 different phosphorus-based electrolytes, comprising a total of 1740 combinations. A yellow background indicates that the color of graphite in the Li/Gr test electrode turned gold after soaking in the respective electrolyte. (b) P:Li molar ratio of the relevant phosphorus-based electrolytes used in (a). (c) The desolvation energy of a Li+ with four molecules of phosphorus-based solvents and carbonate solvent by DFT calculation.

2.2 Further electrolyte screening: Li/GR half-cell and Gr/LFP fuel cell

Galvanostatic charge/discharge of coin cells with Li/Gr half cell and Gr/LFP full cell configurations are utilized to further narrow down the range of good combinations from the initial 101 positive results obtained through the HTP screening. Figure 3a and Figure S3 illustrate the 1st charge/discharge curves of Li/Gr half-cells at 0.02 C for the 101 positive combinations screened by the HTP method. Among these, 26 combinations exhibited a reversible specific capacity higher than 320 mAh/g (Fig. 3b, and Figure S4), which is close to the graphite in the standard carbonate electrolyte (Fig. S1g) and are considered potential candidates for Gr/LFP full cell evaluation. The remaining 75 combinations showed low reversible capacity, less than 320 mAh/g, in the Li/Gr half cells. Out of these, approximately 21 combinations (Fig. S5a) exhibited a reversible capacity of less than 100 mAh/g. The reason these 21 combinations still presented positive results/color change in the HTP screening is attributed to the differences in the electrochemical processes between the Li/Gr test electrode in the HTP screening and the Li/Gr coin cell testing. In the Li/Gr test electrode of the HTP screening, there is the lowest resistance (short circuit) due to the direct connection of Li and graphite by Cu foil, and the absence of a separator (Fig. 1e), leading to a fast dynamic response. However, when tested in a Li/Gr coin cell, the cell's constant current operation at 0.02 C or above, along with the presence of a porous separator, results in larger cell impedance and slower dynamics, thereby leading to low capacity. If the Li/Gr coin cells of these 21 combinations were wrapped with Cu foil for 24 hours to simulate the short circuit in the Li/Gr test electrode, the reversible capacity of all 21 combinations increased to above 100 mAh/g, with some exceeding 250 mAh/g (Fig. S5b). Disassembling the shorted Li/Gr coin cell, such as S29A2 (Gr#2 and 1.2 M LiFSI TEP + 10% 1,3-PS) with the lowest specific capacity of 104.6 mAh/g, the graphite electrode displayed partial gold coloration (Fig. S5c), which is consistent with the HTP screening results. Thus, Li/Gr coin cell testing can further narrow down the range of positive results obtained from HTP screening.Among the 26 potential combinations with reversible specific capacity over 320 mAh/g (Fig. 3b), Gr#5 was observed in eight out of the 26 combinations. Additionally, at low concentrations of 1.2 M phosphorus-based electrolytes, only Gr#5 (S16A35) and Gr#3 (S29A15) in 1.2 M LiDFOB TBP + 10% VEC and 1.2 M LiFSI TEP + 10% FEC, respectively, displayed a reversible capacity of ~330 mAh/g with 91.3% and 70.7% of initial CE, as shown in Figure. S6. Considering high CE and its compatibility, Gr#5 having 10-20 µm particle size (Fig. S1e) was selected as the graphite anode for further electrolyte screening. In the Gr/LFP cells with an areal capacity of ~2.9 mAh/cm2, the cell with 1.2 M LiDFOB TBP + 10% VEC delivered only 64.3 mAh/g at 0.1 C and 5.9 mAh/g at 0.33 C (Fig. 3c and Fig. S7a). Even at 0.02 C, the cell delivered only 106.3 mAh/g (Fig. S7b) due to the high desolvation energy of -90.1 kcal/mol (Fig.2c), high viscosity of 20.4 cP at 25 °C and low ionic conductivity of 2.17 mS/cm at 25 °C (Fig. 3d), as well as the use of commercial-level thick electrodes. In 2 M LiFSI TEP + 10% FEC (S36A17), Gr#5 delivered similar cell performance, with 333.7 mAh/g of specific capacity and 89.0% of initial CE, as observed in 1.2 M LiDFOB TBP + 10% VEC in Li/Gr half-cell testing. Despite the high viscosity of 16.8 cP at 25 °C and low ionic conductivity of 3.45 mS/cm at 25 °C, in comparison with 3.6 cP and 7.54 mS/cm of the carbonate electrolyte (Fig. 3d), the Gr/LFP cell in 2 M LiFSI TEP + 10% FEC delivered 141.3 mAh/g at 0.1 C (Fig. 3c), similar to the 146.4 mAh/g obtained with the carbonate electrolyte, indicating a good SEI on Gr#5. However, increasing the rate to 0.33 C in the cell with 2 M LiFSI TEP + 10% FEC resulted in a long constant voltage (CV) charge plateau at 3.8 V (~39% of the capacity) during the charge process and larger voltage polarization, leading to a low specific capacity of 129.9 mAh/g compared to 142.3 mAh/g in the carbonate electrolyte. The reason behind this is the large desolvation energy between Li+ and TEP (Fig. 2c), which is -62.5 kcal/mol, 5 times higher than that of the carbonate electrolyte, making it difficult for Li+ to disengage from the TEP solvents.

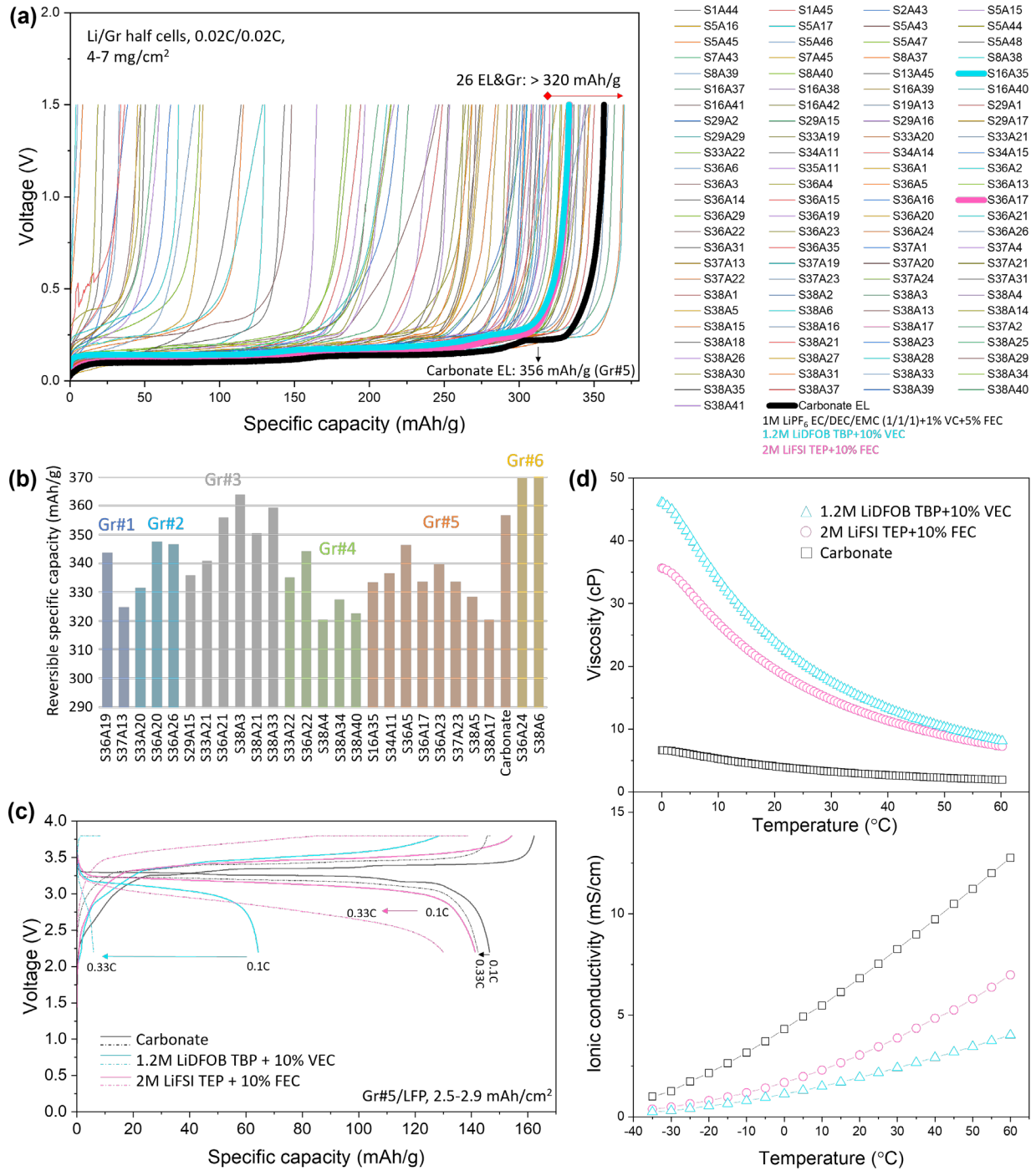

Figure 3. Further electrolytes screening in Li/Gr half cells and Gr/LFP full cells. (a) The 1st charge curves of Li/Gr half cells at 0.02 C for the 101 positive combinations screened by the HTP method in Figure 2a. Working voltage: 0-1.5 V. (b) 26 potential combinations among 101 positive combination in (a) that exhibit an initial reversible specific capacity exceeding 320 mAh/g. (c) The voltage profiles of Gr#5/LFP cells in two identified phosphorus-based electrolytes and a carbonate electrolyte at 0.1 C (real line) and 0.33 C (dash line). Working voltage: 2.2-3.8 V. (d) The relationships of viscosity (top)/ionic conductivity (bottom) and temperature of the three electrolytes in (c).

2.3 Electrolyte optimization

To enhance the cell performance of Gr/LFP cells in 2 M TEP electrolyte at 0.33 C, the addition of cosolvents is considered to decrease the molar ratio of P:Li, thereby reducing the number of TEP phosphate solvent that need to be eliminated during the charge process. The selection of a low viscosity cosolvent can contribute to decreasing the overall electrolyte viscosity and increasing the ionic conductivity, thereby facilitating faster ionic transportation. The chosen cosolvent should meet the following criteria: 1) low viscosity (η), 2) high dielectric constant (ε), and 3) maintenance of non-flammability of TEP electrolyte at the maximum addition. Potential cosolvents include dimethoxyethane (DME) with a low η of 0.48 cP at 20 °C and ethylene carbonate (EC) with a high ε of 95.3 at 25 °C, as reported in the literature.[31] As observed in Figure.4a, gradually increasing the volume ratio of DME and EC in TEP electrolyte results in a continuous decrease in viscosity and a continuous increase in ionic conductivity. In particular, in 2 M LiFSI TEP/DME/EC (6/2/2, v/v/v) + 5% FEC + 5% VEC, the viscosity drops to 7.6 cP, while the ionic conductivity reaches 7.67 mS/cm, comparable to the carbonate electrolyte. Even at -35 °C, the ionic conductivity remains at 0.93 mS/cm, which is comparable to the 1.0 mS/cm observed in the carbonate electrolyte. Additionally, when exposed to fire, the 2 M LiFSI TEP/DME/EC (6/2/2, v/v/v) + 5% FEC + 5% VEC electrolyte is hard to ignite, and any small fire that occurs is extinguished within a second. In contrast, the carbonate electrolyte displayed continuous burning. It is important to note that reducing the volume ratio of TEP to 50% made the electrolyte flammable and was therefore not considered for further study. Furthermore, the molar ratio of P:Li in 2 M LiFSI TEP/DME/EC (6/2/2, v/v/v) + 5% FEC + 5% VEC is also decreased to 1.8:1, which is lower than the 2.9:1 observed in 2 M LiFSI TEP + 10% FEC (Fig.2b), contributing to a faster dynamic response due to fewer TEP molecules. In Gr#5/LFP full cell tests with an areal capacity of 2.9 mAh/cm2, the cell with 2 M LiFSI TEP/DME/EC (6/2/2, v/v/v) + 5% FEC + 5% VEC demonstrated an impressive performance, cycling 140 times at 80% of end-of-life (EOL) and 200 times at 70% of EOL at 0.33 C/0.33 C. This is a significant improvement compared to the 2 M LiFSI TEP + 10% FEC, which cycled only 200 times at 40% of EOL (Fig.4b and Fig.S8a). Additionally, the 2 M LiFSI TEP/DME/EC (6/2/2, v/v/v) + 5% FEC + 5% VEC electrolyte did not exhibit a long CV charge plateau at 0.33 C during the cycling process (Fig.S8b and S8c), unlike the 2 M LiFSI TEP + 10% FEC (Fig.S8d), indicating an improvement in dynamic performance through the addition of DME and EC. Furthermore, apart from the low flammability of the 2 M LiFSI TEP/DME/EC (6/2/2, v/v/v) + 5% FEC + 5% VEC electrolyte, its thermal stability with fully lithiated graphite (Gr#5, 100% SOC) is also enhanced compared to the carbonate electrolyte. This is evident as the fully lithiated Gr#5 in the carbonate electrolyte presents a four times higher exothermic peak at 258 °C compared to the 2 M LiFSI TEP/DME/EC (6/2/2, v/v/v) + 5% FEC + 5% VEC (Fig.4c), proving the intrinsically safe properties of the developed TEP electrolyte. Additionally, the cycling performance with commercial-level graphite and LFP electrodes in the TEP-dominant electrolyte in this study outperforms the phosphate-dominant electrolyte reported in previous studies (Fig.4d). Simply replacing DME with other low-viscosity solvents commonly used in LIB, such as DMC, EP, and TTE, did not result in good cycling performance as observed with DME (Fig.S9a and S9b). All the cells with DMC, EP, and TTE cosolvents experienced rapid fading and retained only 40%-48% of EOL after 200 cycles at 0.33 C. However, when cycled at 0.1 C, all the cells with DMC, EP, and TTE cosolvents displayed stable cycling, retaining 89-96% of EOL after 100 cycles, comparable to the 93% of EOL observed in the carbonate electrolyte (Fig.S9c and S9d). This suggests a thermodynamically stable behavior between these electrolytes and graphite. Nonetheless, it is crucial to re-tune the ratio of DMC, EP, or TTE, SEI additives, and other cosolvents for optimal dynamic performance in DMC, EP, or TTE type TEP electrolytes, which will be a subject of future research using HTP screening technology. Moreover, other potential combinations from the HTP screening were also tried with the addition of DME/EC cosolvents

derived from S36A17 (Gr#5 and 2 M LiFSI TEP + 10% FEC), such as S34A11, S36A5, S36A23, which had the same Gr#5 (Fig.S10), and S36A24, S38A3, S38A6, S38A33, which had different graphite materials (Fig.S4). However, none of these combinations demonstrated good cycling performance after the addition of DME/EC to the respective phosphorus-based electrolytes (Fig.S11a and S11b), indicating that the optimized recipe for a potential combination is not universally applicable to other combinations. Different potential combinations of graphite material and phosphorus-based electrolyte may require their own cosolvents and SEI additives, which will be incorporated into the next HTP screening.

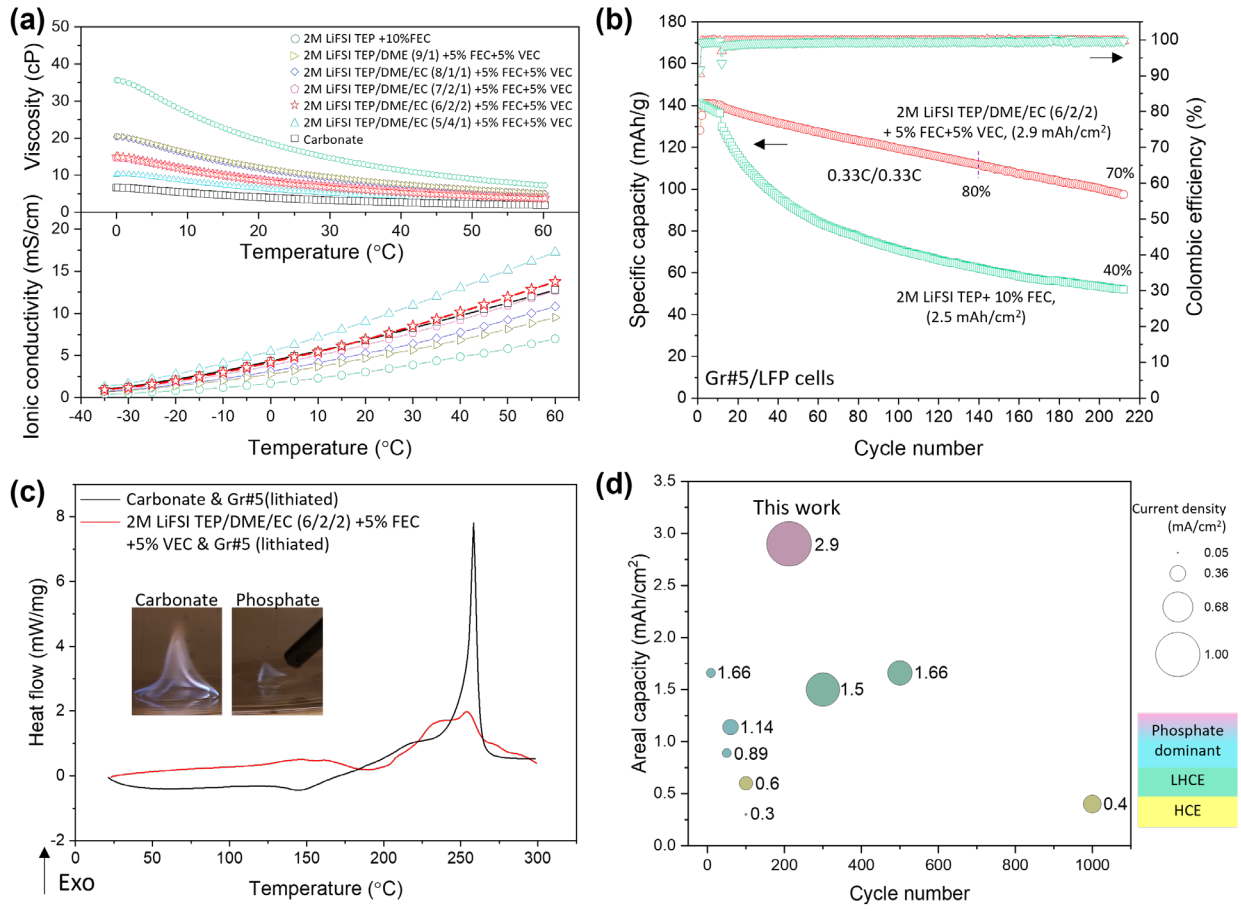

Figure 4. Electrolyte optimization with addition of cosolvents. (a) The relationship of viscosity (top)/ionic conductivity (bottom) varied with temperature of TEP-based electrolytes with different cosolvents and carbonate electrolyte. (b) Cycling performance of Gr#5/LFP cells in 2 M LiFSI TEP/DME/EC (6/2/2, v/v/v) + 5% FEC + 5% VEC (red) and 2 M LiFSI TEP + 10% FEC (green) at 0.33 C/0.33 C. Formation: 0.1 C/0.1 C for 11 cycles. (c) The DSC thermal stability test of fully lithiated graphite Gr#5 in 2 M LiFSI TEP/DME/EC (6/2/2, v/v/v) + 5% FEC + 5% VEC (red) and carbonate baseline electrolyte (black). Inset: flammability test of the two electrolytes used in DSC test. (d) A summary of previous works related to phosphorus-based electrolytes and a comparison to this work. The ball size represents current density.

3.0 References

1. J. Liu, J. Xiao, J. Yang, W. Wang, Y. Shao, P. Liu and M. S. Whittingham, Next Energy, 2023, 1, 100015.
2. J. Liu, Z. Huang, M. Fan, J. Yang, J. Xiao and Y. Wang, Nano Energy, 2022, 104, 107915.
3. C. F. Heuberger and N. Mac Dowell, Joule, 2018, 2, 367-370.
4. P. Sturm, P. Fößleitner, D. Fruhwirt, S. F. Heindl, O. Heger, R. Galler, R. Wenighofer and S. Krausbar, Data in Brief, 2023, 46, 108839.
5. J. Sun, B. Mao and Q. Wang, Fire Safety Journal, 2021, 120, 103119.
6. X. Wang, E. Yasukawa and S. Kasuya, Journal of The Electrochemical Society, 2001, 148, A1058.
7. K. Xu, M. S. Ding, S. Zhang, J. L. Allen and T. R. Jow, Journal of The Electrochemical Society, 2002, 149, A622.
8. J. Chen, A. Naveed, Y. Nuli, J. Yang and J. Wang, Energy Storage Materials, 2020, 31, 382-400.
9. X. L. Yao, S. Xie, C. H. Chen, Q. S. Wang, J. H. Sun, Y. L. Li and S. X. Lu, Journal of Power Sources, 2005, 144, 170-175.
10. L. Jiang, C. Liang, H. Li, Q. Wang and J. Sun, ACS Applied Energy Materials, 2020, 3, 1719-1729.
11. H. F. Xiang, Q. Y. Jin, C. H. Chen, X. W. Ge, S. Guo and J. H. Sun, Journal of Power Sources, 2007, 174, 335-341.
12. X. Cao, Y. Xu, L. Zhang, M. H. Engelhard, L. Zhong, X. Ren, H. Jia, B. Liu, C. Niu, B. E. Matthews, H. Wu, B. W. Arey, C. Wang, J.-G. Zhang and W. Xu, ACS Energy Letters, 2019, 4, 2529-2534.
13. S. Takeuchi, S. Yano, T. Fukutsuka, K. Miyazaki and T. Abe, Journal of The Electrochemical Society, 2012, 159, A2089.
14. H. F. Xiang, J. Y. Shi, X. Y. Feng, X. W. Ge, H. H. Wang and C. H. Chen, Electrochimica Acta, 2011, 56, 5322-5327.
15. X. Wang, C. Yamada, H. Naito, G. Segami and K. Kibe, Journal of The Electrochemical Society, 2006, 153, A135.
16. P. Shi, H. Zheng, X. Liang, Y. Sun, S. Cheng, C. Chen and H. Xiang, Chemical Communications, 2018, 54, 4453-4456.
17. Z. Zeng, V. Murugesan, K. S. Han, X. Jiang, Y. Cao, L. Xiao, X. Ai, H. Yang, J.-G. Zhang, M. L. Sushko and J. Liu, Nature Energy, 2018, 3, 674-681.
18. H. Jia, Z. Yang, Y. Xu, P. Gao, L. Zhong, D. J. Kautz, D. Wu, B. Fliegler, M. H. Engelhard, B. E. Matthews, B. Broekhuis, X. Cao, J. Fan, C. Wang, F. Lin and W. Xu, Advanced Energy Materials, 2023, 13, 2203144.
19. S. Matsuda, K. Nishioka and S. Nakanishi, Scientific Reports, 2019, 9, 6211.

20. Benayad, A., D. Diddens, A. Heuer, A. N. Krishnamoorthy, M. Maiti, F. L. Cras, M. Legallais, F. Rahmanian, Y. Shin, H. Stein, M. Winter, C. Wölke, P. Yan and I. Cekic-Laskovic, Advanced Energy Materials, 2022, 12, 2102678.
21. J. T. Yik, L. Zhang, J. Sjölund, X. Hou, P. H. Svensson, K. Edström and E. J. Berg, Digital Discovery, 2023, DOI: 10.1039/D3DD00058C.
22. O. Borodin, M. Olguin, C. E. Spear, K. W. Leiter and J. Knap, Nanotechnology, 2015, 26, 354003.
23. L. Su, M. Ferrandon, J. A. Kowalski, J. T. Vaughey and F. R. Brushett, Journal of The Electrochemical Society, 2014, 161, A1905.
24. H. J. Y. Liang, R. Feng, F. Parks, X. Zhang, A. Hollas, M. Bowden, V. Murugesan, W. Wang, , ChemRxiv (2023). , 2023, This content is a preprint and has not been peer-reviewed. 10.26434/chemrxiv-22023-26985h26437.
25. C. R. Birkl, M. R. Roberts, E. McTurk, P. G. Bruce and D. A. Howey, Journal of Power Sources, 2017, 341, 373-386.
26. C. Täubert, M. Fleischhammer, M. Wohlfahrt-Mehrens, U. Wietelmann and T. Buhrmester, Journal of The Electrochemical Society, 2010, 157, A721.
27. L. Xia, S. Lee, Y. Jiang, Y. Xia, G. Z. Chen and Z. Liu, Journal, 2017, 2, 8741-8750.
28. X. Chen, N. Yao, B.-S. Zeng and Q. Zhang, Fundamental Research, 2021, 1, 393-398.
29. J. Wang, Y. Yamada, K. Sodeyama, E. Watanabe, K. Takada, Y. Tateyama and A. Yamada, Nature Energy, 2018, 3, 22-29.
30. X. Fan, X. Ji, L. Chen, J. Chen, T. Deng, F. Han, J. Yue, N. Piao, R. Wang, X. Zhou, X. Xiao, L. Chen and C. Wang, Nature Energy, 2019, 4, 882-890.
31. S. I. Tobishima, J. I. Yamaki and T. Okada, Electrochimica Acta, 1984, 29, 1471-1476.

Appendix A – Supplementary Information

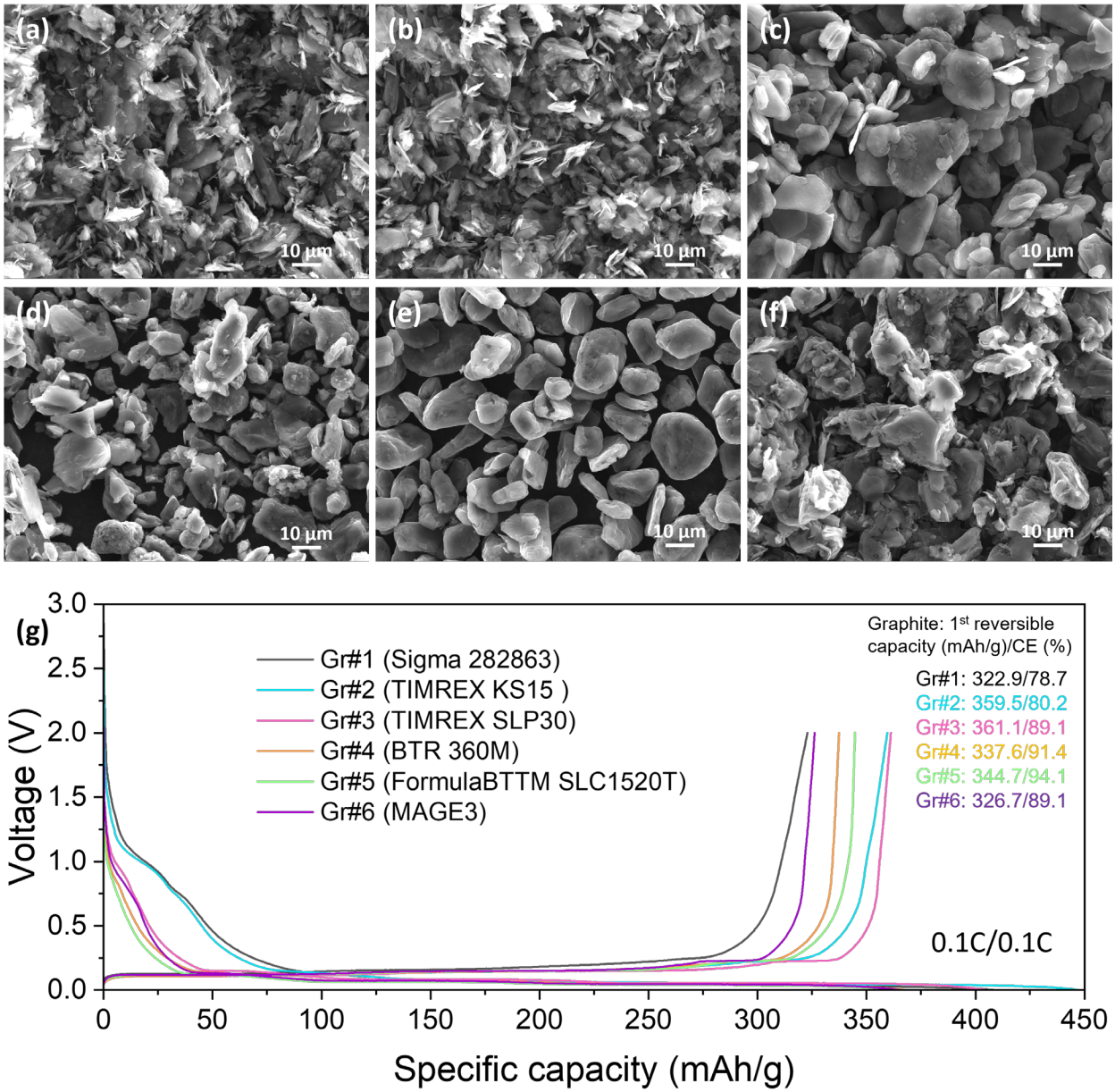

Figure S1. The properties of six graphite materials utilized in HTP screening. (a-f) The morphology of six commercially available graphite materials by SEM: (a) 282863 (Sigma-Aldrich, Gr#1), (b) TIMREX KS15 (TIMCAL, Gr#2), (c) TIMREX SLP30 (TIMCAL, Gr#3), (d) S360-M (BTR, Gr#4), (e) FormulaBTTM SLC1520T (Superior Graphite, Gr#5), and (f) Mage 3 (Hitachi, Gr#6). (g) The 1st voltage profiles of Li/Gr half cells with six graphite anode materials in carbonate baseline electrolytes at 0.1 C/ 0.1 C. Working voltage: 0-1.5 V.

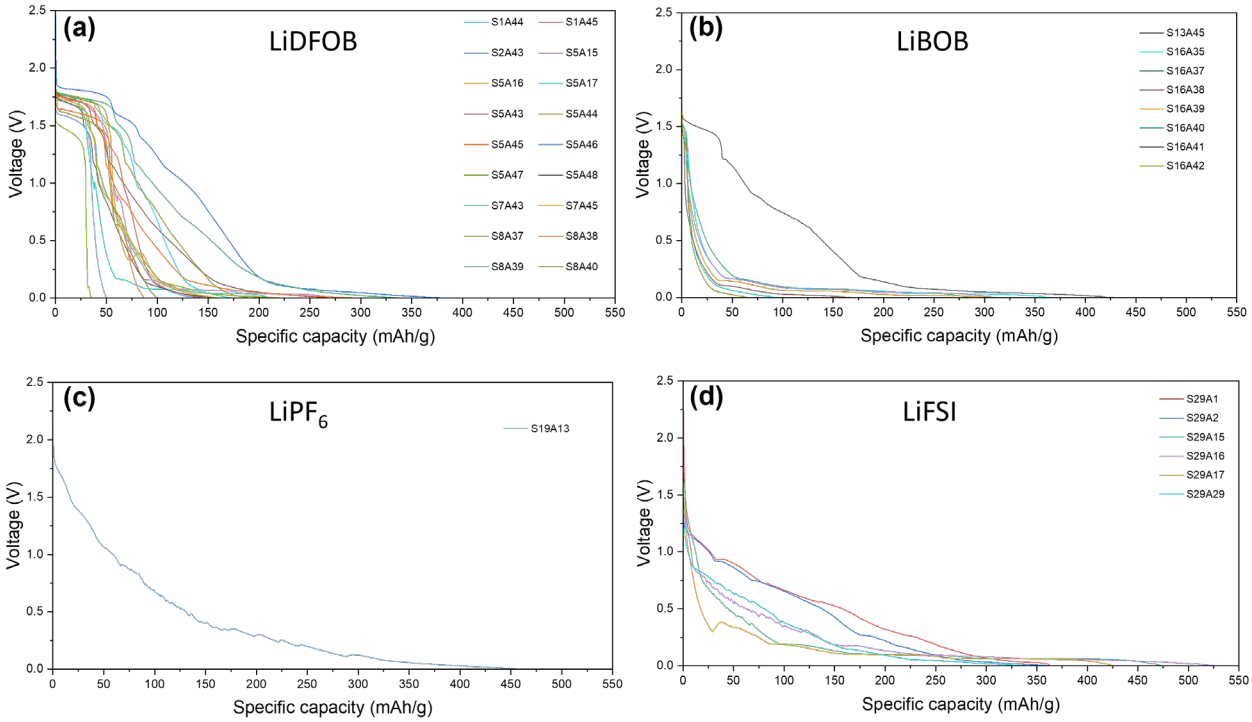

Figure S2. The effect of lithium salts in phosphorous-based electrolyte. (a-d) The 1st discharge profiles of Li/Gr half cells at 0.02 C in phosphorus-based electrolytes with various lithium salts: (a) LiDFOB, (b) LiBOB, (c) LiPF6 and (d) LiFSI. These voltage profiles were extracted from Figure S3.

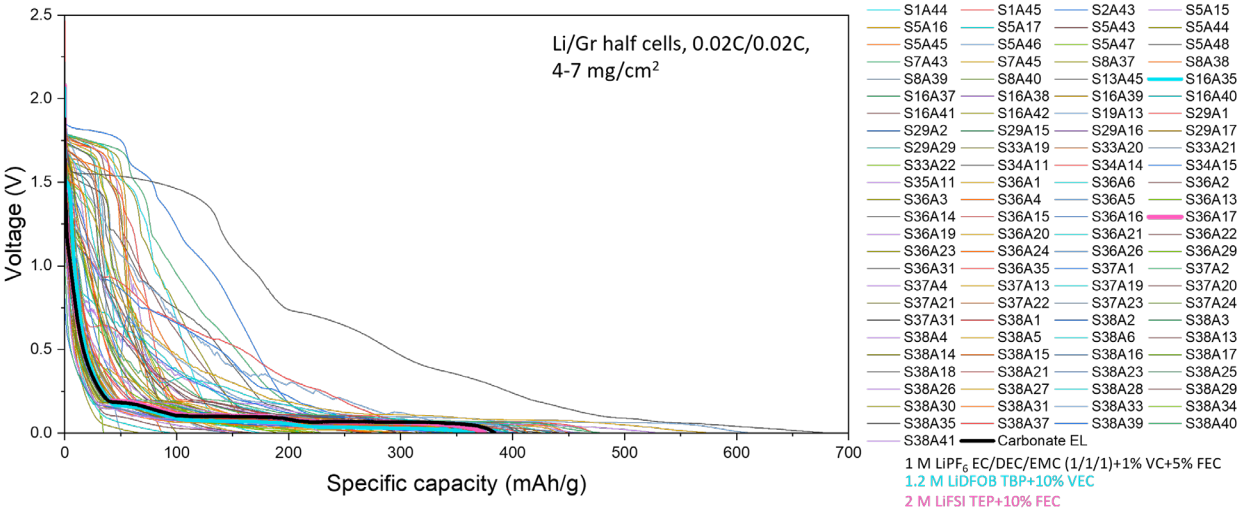

Figure S3. Further electrolyte screening in Li/Gr half cells. The 1st discharge curves of Li/Gr half cells at 0.02 C for the 101 positive combinations screened by the HTP method in Figure 2a. Working voltage: 0-1.5 V.

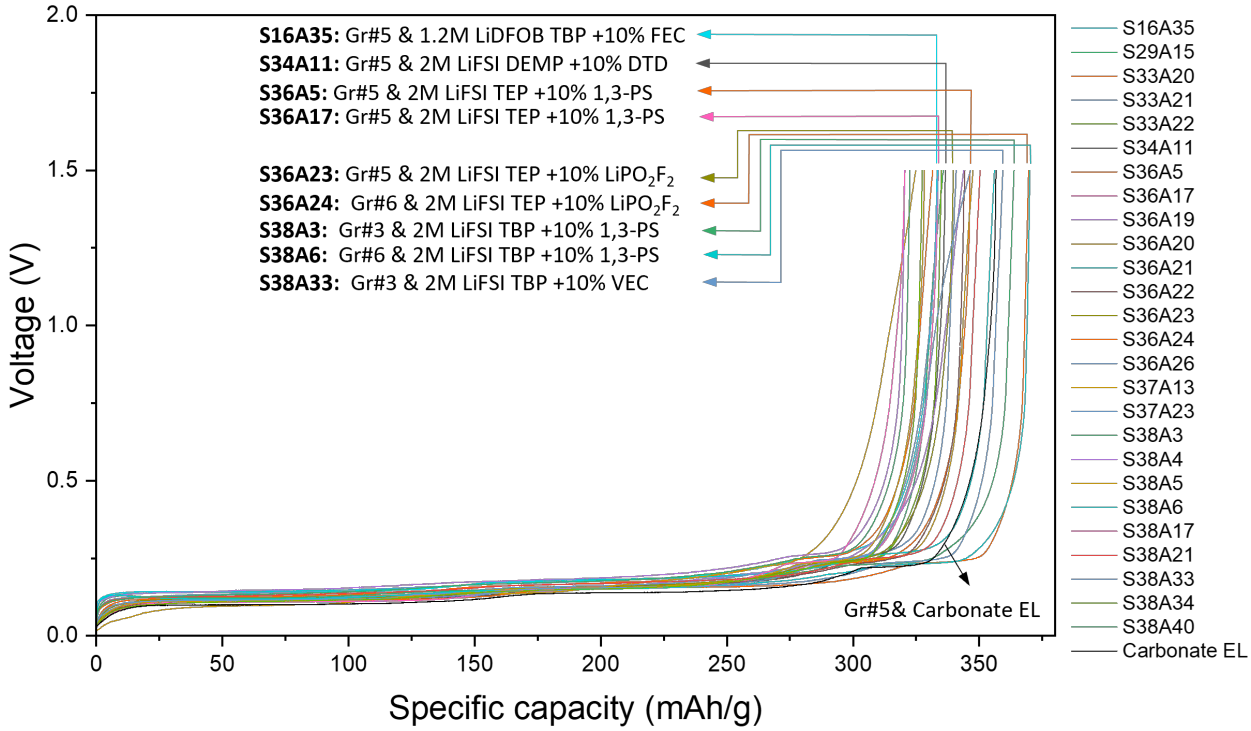

Figure S4. 1st charge profiles of 26 potential combinations among 101 positive combinations in Fig.3a that exhibit an initial reversible specific capacity exceeding 320 mAh/g. Some promising combinations discussed in following main text were listed.

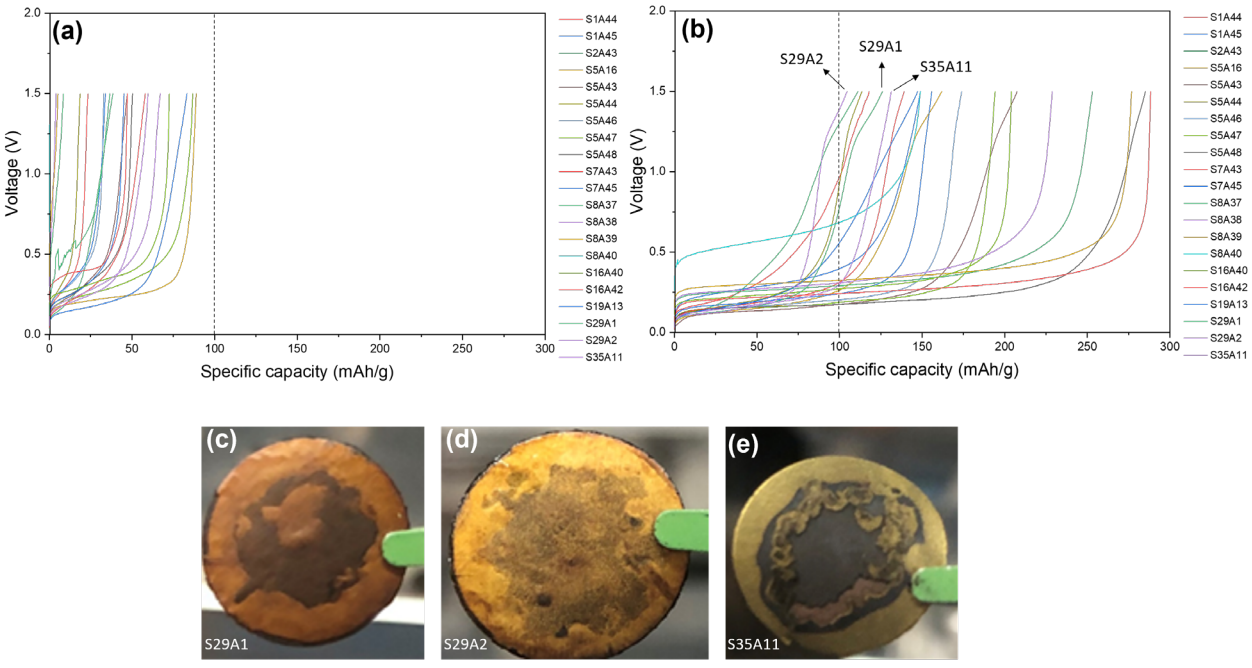

Figure S5. Short circuit study of Li/Gr half cells. (a) 1st charge profiles of 21 combinations exhibited a reversible capacity of less than 100 mAh/g in Li/Gr half cells at 0.02 C in Fig. 3a. (b) 1st charge profiles of Li/Gr half cells in (a) after wrapped the coin cells with Cu foil for 24 hours. (c-d) digital photos of the graphite anode electrodes harvested in shorted coin cells with combinations of (c) S29A1, (d) S29A2 and (e) S35A11.

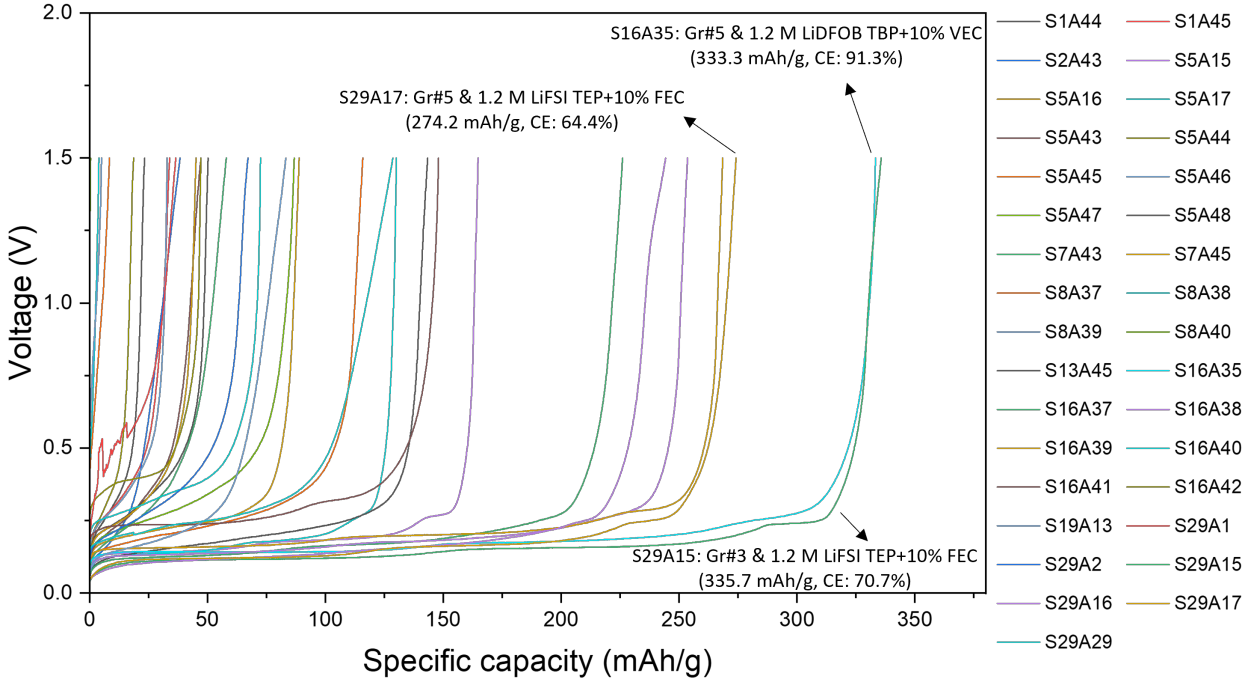

Figure S6. The 1st charge profiles of all positive combinations with low concentration of 1.2M phosphorus-based electrolyte. These charge profiles were extracted from Fig. 3a.

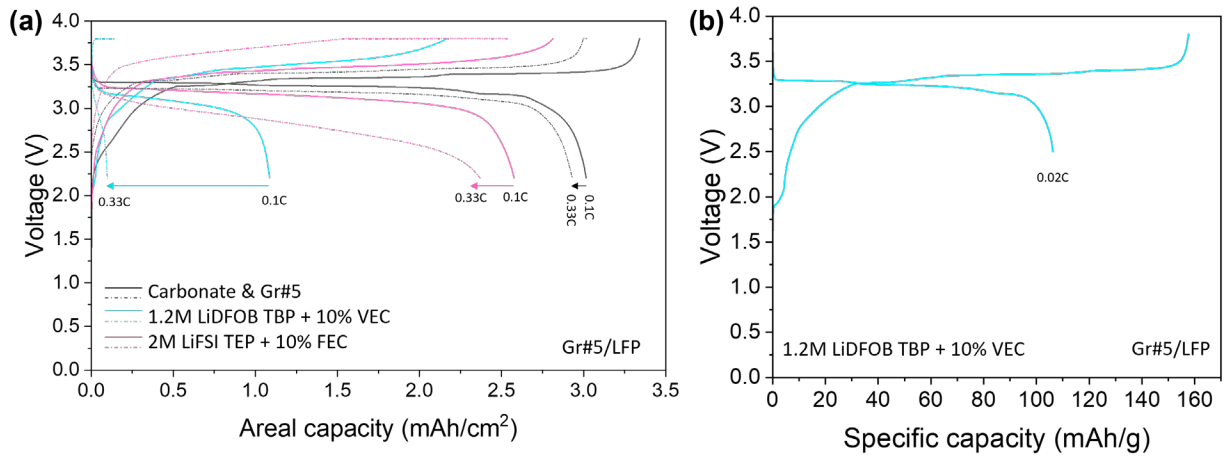

Figure S7. (a) The areal capacity of Gr#5/LFP cells in two identified phosphorus-based electrolytes and a carbonate electrolyte at 0.1 C (real line) and 0.33 C (dash line). Working voltage: 2.2-3.8 V. (b) The 1st voltage profile of Gr#5/LFP cells in 1.2 M LiDFOB TBP + 10% VEC tested at 0.02 C/0.02 C.

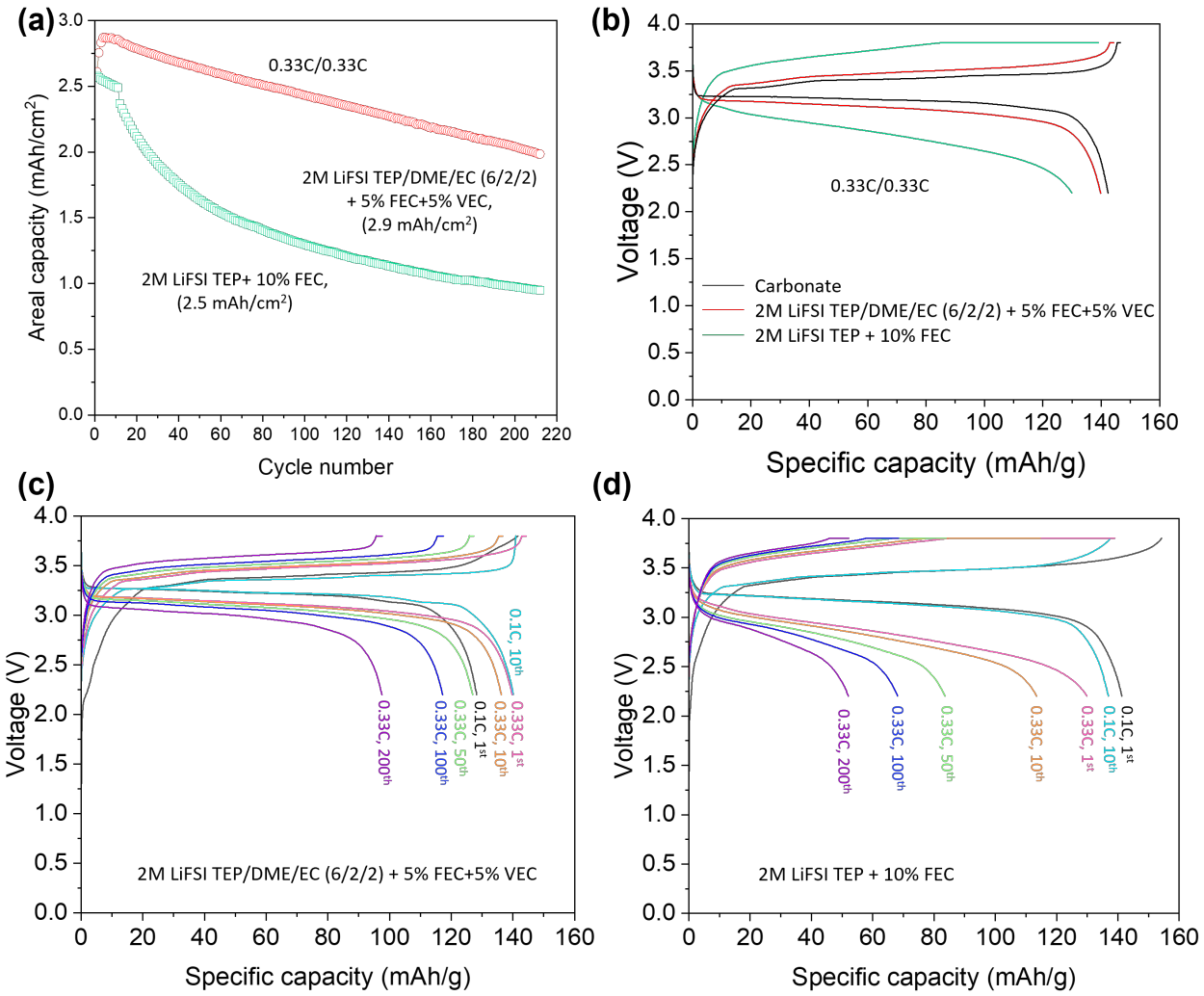

Figure S8. (a) The areal capacity of Gr#5/LFP cells in 2 M LiFSI TEP/DME/EC (6/2/2, v/v/v) + 5% FEC + 5% VEC (red) and 2 M LiFSI TEP + 10% FEC (green) at 0.33 C/0.33 C. Formation: 0.1 C/0.1 C for 11 cycles. (b) The comparison of voltage profiles of Gr#5/LFP cells in three electrolytes at 0.33 C/0.33 C. (c) The voltage profiles of Gr#5/LFP cell at different cycles in 2 M LiFSI TEP/DME/EC (6/2/2, v/v/v) + 5% FEC + 5% VEC. (d) The voltage profiles of Gr#5/LFP cell at different cycles in 2 M LiFSI TEP + 10% FEC.

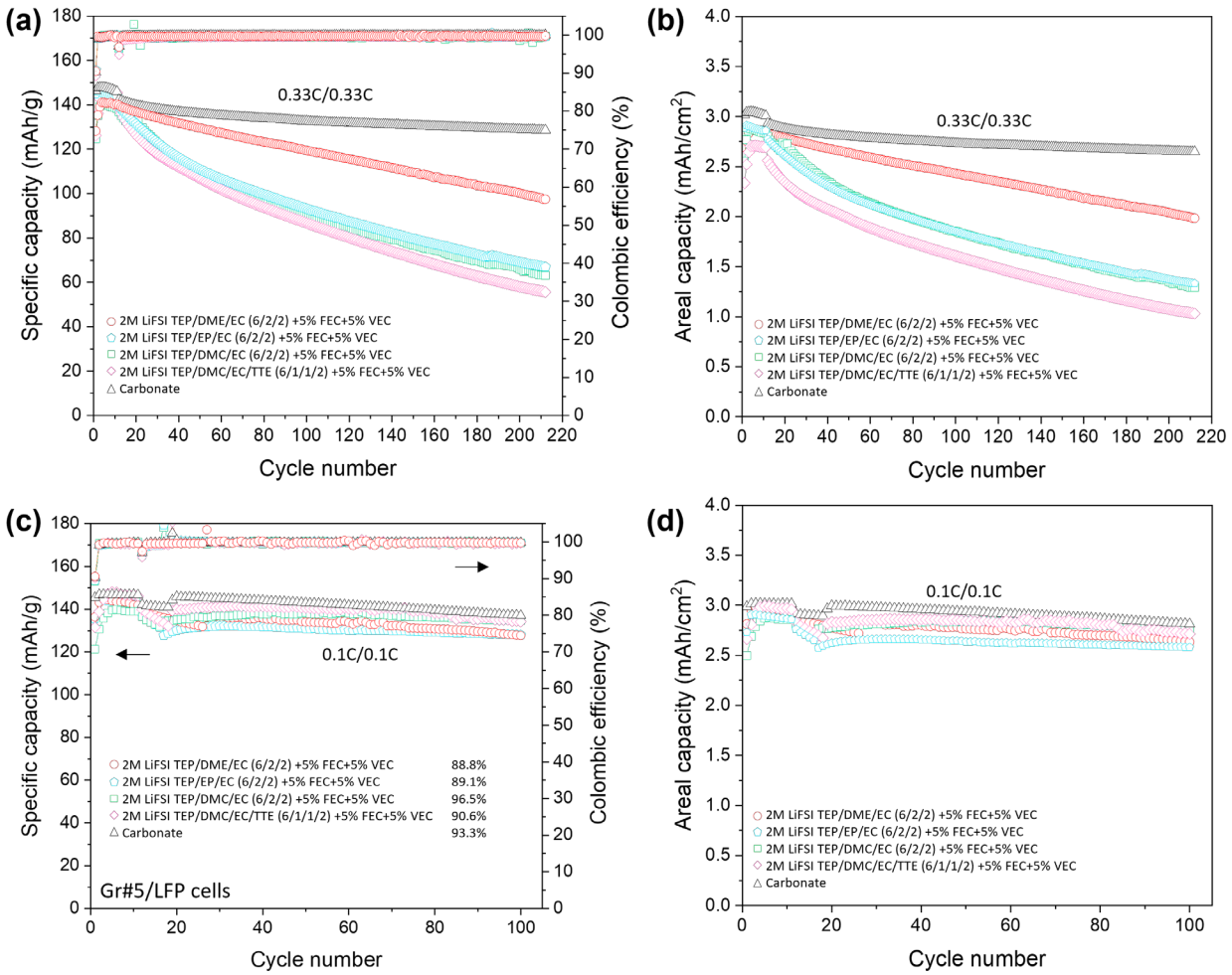

Figure S9. The effect of different cosolvents in electrolyte optimization. (a) The cycling performance of Gr#5/LFP cells in different electrolytes containing different cosolvents at 0.33 C/0.33 C. Formation: 0.1 C/0.1 C for 11 cycles. Working voltage: 2.5-3.8 V. (b) The area capacity of Gr#5/LFP cells tested in (a). (c) The cycling performance of Gr#5/LFP cells in different electrolytes containing different cosolvents at 0.1 C/0.1 C. Formation: 0.1 C/0.1 C for 11 cycles. 5-10 cycles at 0.33 C/0.33 C were performed after formation for consistent check. (d) The area capacity of Gr#5/LFP cells tested in (c).

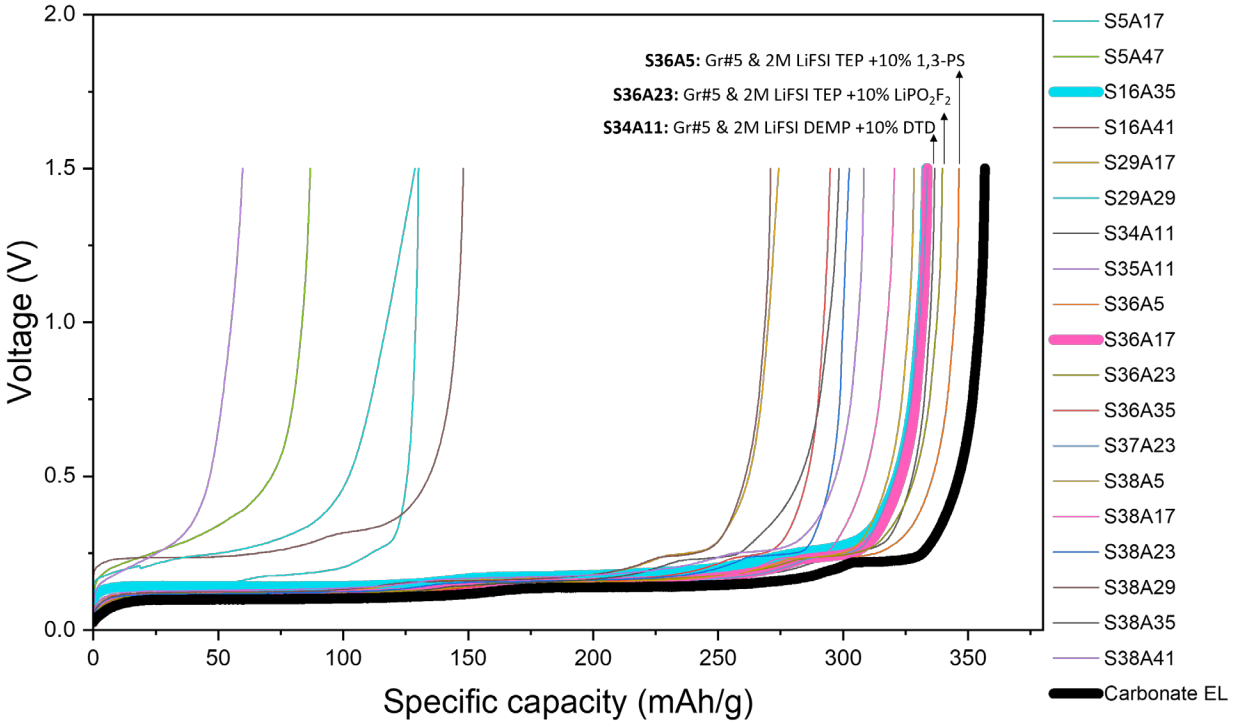

Figure S10. The 1st charge profiles of all positive combinations with Gr#5 as the anode in all Li/Gr half cells. These charge profiles were extracted from Fig. 3a. Three additional combinations were selected for further discussion in main text.

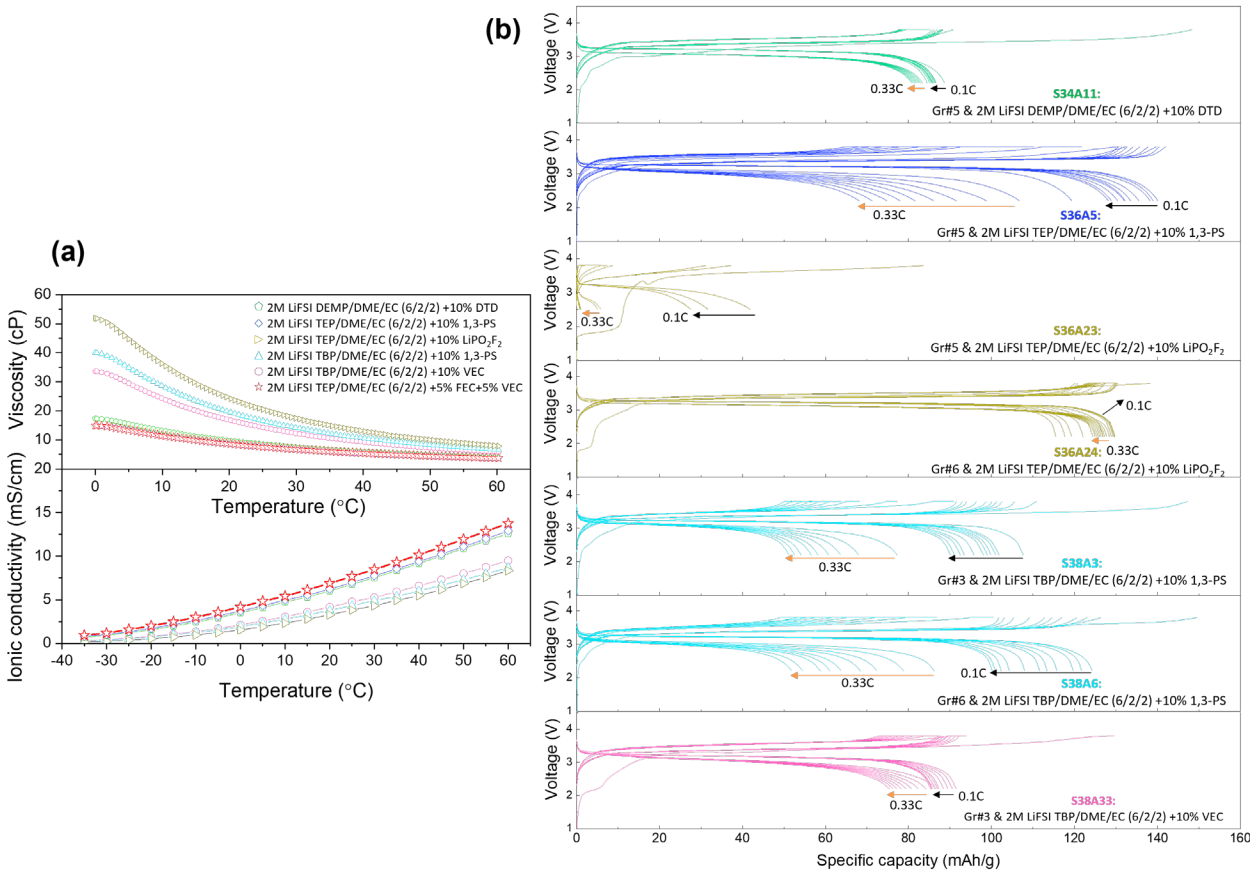

Figure S11. Employment of DME and EC as cosolvents to other potential combinations in Fig. S4. (a) The relationship of viscosity (top)/ionic conductivity (bottom) varied with temperature of different phosphorus-based electrolytes identified in Fig. S4. (b) The voltage profiles of Gr/LFP full cells at different cycles with the graphite and phosphorus-based electrolyte from seven

potential combinations listed in Fig. S4.

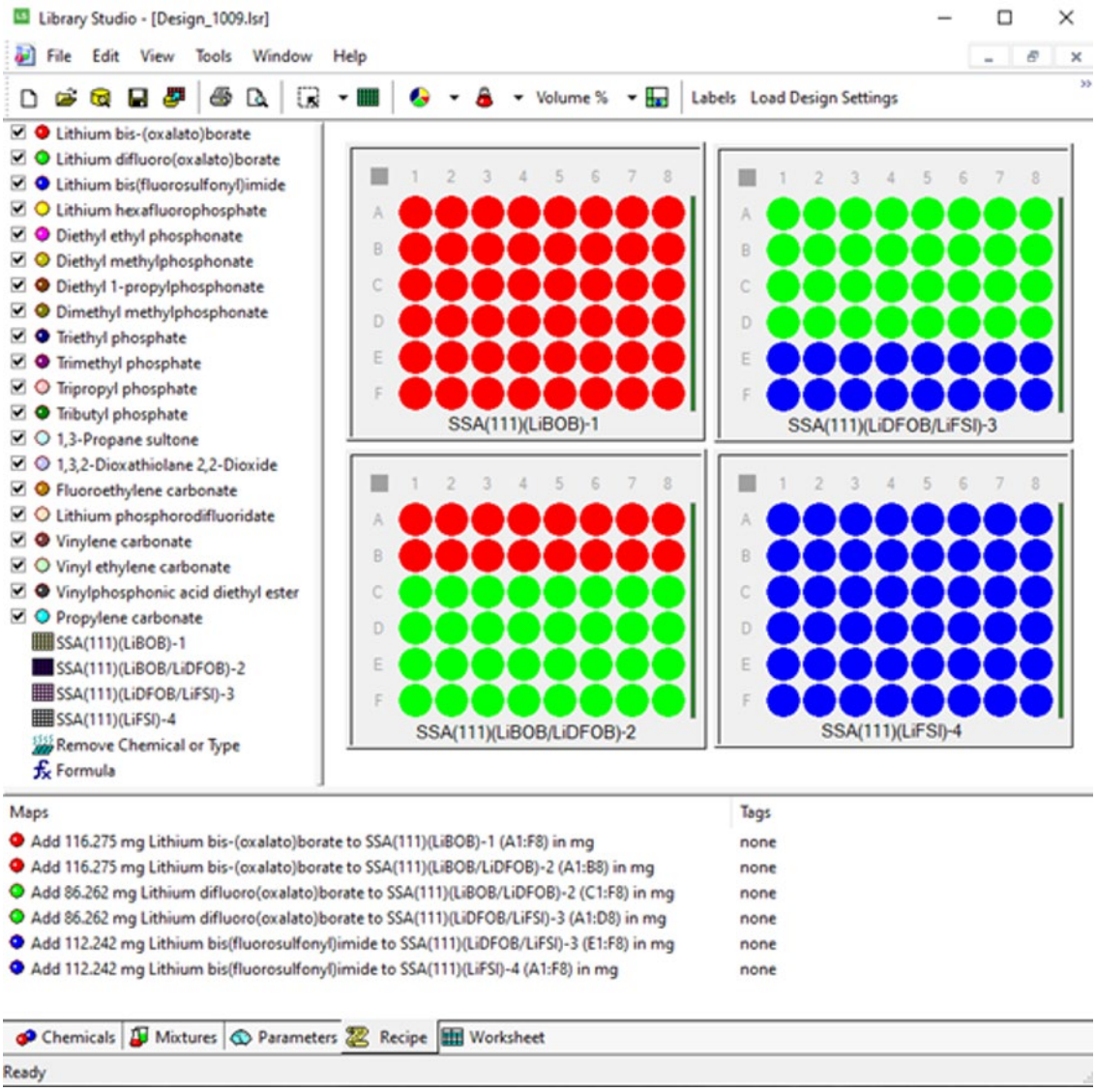

Figure S12. The Laboratory Execution and Analysis (LEA) software suite for HTP electrolyte preparation.

Pacific Northwest National Laboratory

902 Battelle Boulevard
P.O. Box 999
Richland, WA 99354

1-888-375-PNNL (7665)

www.pnnl.gov